Screening effects on $^{12}C+^{12}C$ fusion reaction *

F. Koyuncu[1)] A. Soylu

Department of Physics, Nigde Ömer Halisdemir University, 51240, Nigde, Turkey

Abstract: One of the important reactions for nucleosynthesis in the carbon burning phase in high-mass stars is the $^{12}C+^{12}C$ fusion reaction. In this study, we investigate the influences of the nuclear potentials and screening effect on astrophysically interesting $^{12}C+^{12}C$ fusion reaction observables at sub-barrier energies by using the microscopic $\alpha-\alpha$ double folding cluster (DFC) potential and the proximity potential. In order to model the screening effects on the experimental data, a more general exponential cosine screened Coulomb (MGECSC) potential including Debye and quantum plasma cases has been considered in the calculations for the $^{12}C+^{12}C$ fusion reaction. In the calculations of the reaction observables, the semi-classical Wentzel-Kramers-Brillouin (WKB) approach and coupled channel (CC) formalism have been used. Moreover, in order to investigate how the potentials between ^{12}C nuclei produce molecular cluster states of ^{24}Mg, the normalized resonant energy states of ^{24}Mg cluster bands have been calculated for the DFC potential. By analyzing the results produced from the fusion of $^{12}C+^{12}C$, it is found that taking into account the screening effects in terms of MGECSC is important for explaining the $^{12}C+^{12}C$ fusion data, and the microscopic DFC potential is better than the proximity potential in explaining the experimental data, also considering that clustering is dominant for the structure of the ^{24}Mg nucleus.

Keywords: nuclear fusion, nucleosynthesis, screening effects, clustering, potential model

PACS: 26.20.-f, 25.70.Jj **DOI:** 10.1088/1674-1137/42/5/054106

1 Introduction

Stars have different characteristics and one of the most important features of stars is their mass. Depending on the mass, the types and time periods of the different stages of burning in the core of the star change. The lifetime of the star is shortened but there is an increase in the number of synthesized nuclei. Main sequence stars burn their hydrogen (H) to helium (He) via various reaction channels [1, 2]. After each burning phase the core of the star contracts, the temperature in the core rises, and the products of the last stage start to burn. With the end of the helium burning phase, ^{12}C and ^{16}O become the most abundant nuclei in the core. A new contraction rises the temperature to the level where carbon burning can occur [3–5]. If the mass of the star is between $9M_{\odot} \leqslant M \leqslant 11M_{\odot}$, carbon burning occurs as the final stage [5] and if it is more massive than $11M_{\odot}$, neon, oxygen and silicon burning stages can also occur. In the carbon burning phase, the $^{12}C+^{12}C$ fusion reaction plays a major role in nucleosynthesis. Therefore, studies performed on this reaction have became one of the most active fields in nuclear astrophysics. So far $^{12}C+^{12}C$ fusion reaction observables have been investigated experimentally and theoretically, and studies on measuring the cross-section have been reached almost 2 MeV [6–18]. Typically the temperature of the carbon burning phase is in the range 0.8 to 1.0 or 1.2 GK, which corresponds to 1-3 MeV center-of-mass energies [14, 19, 20]. The Coulomb barrier for $^{12}C+^{12}C$ fusion is approximately 6.3 MeV, so astrophysical energies are far below the Coulomb barrier and unfortunately this makes it difficult to measure the cross sections of the fusion reaction.

Recently, different approaches and nuclear potentials have been used in theoretical calculations to give better explanations of the experimental data for the $^{12}C+^{12}C$ fusion reaction [20–28]. One useful method to calculate the fission, fusion and capture reaction observables is the semi-classical Wentzel-Kramers-Brillouin (WKB) approach [27–32]. Haider et al. studied astrophysically interesting reactions of $^{12}C+^{12}C$, $^{12}C+^{16}O$, $^{16}O+^{16}O$ at sub-barrier energies. They have used the proximity potential to obtain the observables of the mentioned fusion reactions with the WKB approximation and Hill-Wheeler formula [28, 33]. The $^{12}C+^{12}C$ fusion reaction together with deformation case of ^{12}C nuclei has been investigated in the framework of the WKB method in Ref. [27]. Besides the semi-classical approaches, the coupled-

Received 4 January 2018, Revised 5 March 2018, Published online 16 April 2018

∗ Supported by the Turkish Science and Research Council (TÜBİTAK) with (117R015)

1) E-mail: fahrettinkoyuncu85@gmail.com

channel formalism has also been used for the fusion calculations. Elastic scattering cross-sections and S-factor calculations were performed for ^{16}O+^{16}O fusion reaction within the framework of the microscopic $\alpha-\alpha$ double folding cluster (DFC) potential by Kocak et al. and this potential was also used to find the normalized resonant energy states of ^{32}S [34]. Very recently Aziz et al. calculated the astrophysically important ^{12}C+^{12}C, ^{12}C+^{16}O, ^{16}O+^{16}O fusion reactions observables and their reaction rates with the DFC potential [20].

The fusion reactions occuring at sub-barrier energies strictly depend on the quantum tunneling process. Thus any modification to the Coulomb potential because of external factors would affect the cross section and rate of the nuclear reaction. A good example of this is the reactions that occur in stellar plasma. Surrounding nuclei by electron clouds changes the Coulomb potential structure and leads to higher cross sections so the reaction observables need a correction factor f, as shown by Salpeter [36]. With the pioneering work of Salpeter, the screening effects have been studied in various experimental and theoretical studies so far and applied to different astrophysical scenarios such as the pp chain, CNO cycle reactions, and the ^{12}C+^{12}C reaction [36–48, 50, 52, 58]. DeWitt et al. and Graboske et al. made extended studies of the weak, intermediate and strong screening regimes and astrophysical applications of intermediate screenings [40, 41]. Wallace et al. used strong screening corrections for helium burning in an envelope around an accreting neutron star [42]. Dynamic screening of thermonuclear reactions was discussed by Carraro et al. [43]. Gruzinov and Bahcall evaluated the electrostatic screening effects on thermonuclear reaction rates in the Sun [44]. Gasques et al. analyzed the nuclear fusion rates for different nuclear burning regimes and applied their results to the ^{12}C+^{12}C fusion reaction [45]. Famiona et al. investigated relativistic electron-positron plasma screening effect on $A=7$ nuclei induced reactions and showed that screening effects from the relativistic electron-positron plasma are small for reactions which include large Z_1Z_2 values [50]. Dynamical screening effects in the QED (quantum electrodynamical) plasma have been investigated for α-α scattering by Yao et al. and they have reported dynamical screening effects are larger than the static effects [58]. More recently, Chen has used pure and screened Coulomb potentials to analyze the chemical composition configurations of the DBV star PG 0112+104 [52]. On the other hand, Spilateri et al. have proposed the effects of clustering configurations on the quantum tunneling and the cross sections to explain the electron screening puzzle [49]. Besides these sorts of studies, there is also an interest in different screening potentials due to their applications in different area of physics [53–55]. One of these potentials is the more general exponential cosine screened Coulomb potential (MGECSC). This potential allows us to define Debye and quantum plasmas and it has been proposed to investigate the shielding effects on the hydrogen atoms in Debye and quantum plasmas [56, 57].

Building on the above studies, in the present paper, two different types of nuclear potentials (Proximity 77 and DFC) have been used in order to obtain ^{12}C+^{12}C fusion cross sections and astrophysical S factors. For the ^{12}C+^{12}C reaction the weak screening case has been applied and the obtained numerical results from the weak screening condition have been used in the calculations. Thus a direct comparison with experimental data can be made. The MGECSC potential has been used for the astrophysically interesting fusion reaction ^{12}C+^{12}C. In our calculations, we have used the semi-classical WKB approach and coupled-channel formalism to calculate the fusion reaction observables. With the aim of determining whether the produced nuclear potential describes the nuclear structure and reaction observations together, the normalized resonant energy states of ^{24}Mg in terms of the cluster states of ^{12}C+^{12}C have been investigated for the G=16 and 18 cluster bands.

The rest of the paper is organized as follows. In Section 2, we present the theoretical models for the nuclear potentials, the more general exponential cosine screened Coulomb potential and the WKB method. We present and discuss the numerical results in Section 3 and finally give our conclusion in Section 4.

2 Model

Before going beginning the calculations, it is useful to give the potential types that we use. Two different types of nuclear potential were used to describe the interaction between two ^{12}C nuclei. These are the proximity and DFC potentials. In this section, numerical calculations for weak screening case, the MGECSC potential and semi-classical WKB method, are also given.

2.1 Potentials

Proximity potential:

Different types of proximity potential, such as Prox 77, Prox 88, Prox 00 etc, have been used to describe radioactive decays and fusion reaction observables [28, 58–60]. These potentials differ from other phenomenological potentials in terms of adjustable parameters. In this study, the Prox 77 potential has been chosen [60]. According to Prox 77 the nuclear interaction is defined as follows:

$$V_N(\zeta)=4\pi\gamma b\frac{C_1C_2}{C_1+C_2}\phi(\zeta), \tag{1}$$

where $\phi(\zeta)$ is a universal function which depends on the separation between the nuclear surafces as $\zeta=(r-C_1-$

$C_2)/b$, where C_i is the half-central-density radius and $\phi(\zeta)$ is given by

$$\phi(\zeta)=-\frac{1}{2}(\zeta-\zeta_0)^2-0.0852(\zeta-\zeta_0)^3, \qquad \zeta\leqslant\zeta_1 \quad (2)$$

$$=-3.437\exp[-\zeta/0.75], \qquad \zeta>\zeta_1 \quad (3)$$

where ζ_0=2.54, ζ_1=1.2511 and γ=0.9517{1−1.7826[$(N-Z)/A]^2$} is the surface energy coefficient in units of MeV/fm^2. N, Z and A are the total neutron, proton and mass number of the compound system. C_i and R_i are given as follows:

$$\begin{aligned} C_i&=R_i[1-(b/R_i)^2] \\ R_i&=1.28A_i^{1/3}-0.76+0.8A_i^{-1/3}, \end{aligned} \quad (4)$$

where b is the surface width (b was taken to be 1 fm [60]), and A_i is the mass number of the projectile and target nuclei [28, 60].

$\alpha-\alpha$ Double Folding Cluster (DFC) potential:

The double-folding model assumes that the density distribution of two colliding nuclei is normally integrated with respect to the nucleon-nucleon interaction, while in this model, the integral of the alpha-alpha interaction is used to calculate the potential and is as follows:

$$V_N(\boldsymbol{R})=\int\int \rho_{cP}(\boldsymbol{r}_1)\rho_{cT}(\boldsymbol{r}_2)v_{\alpha\alpha}(\boldsymbol{r}_{12})\mathrm{d}\boldsymbol{r}_1\mathrm{d}\boldsymbol{r}_2, \quad (5)$$

where ($\boldsymbol{r}_{12}=\boldsymbol{R}-\boldsymbol{r}_1+\boldsymbol{r}_2$), $v_{\alpha\alpha}(r)$ =-122.6225 exp(-0.22r^2) is the $\alpha-\alpha$ effective interaction potential, and ρ_{cP} and ρ_{cT} are the α densities of the projectile and the target nucleus, respectively [34, 61, 62]. The matter distribution of ^{12}C and the Gaussian form for the α-density distribution can be expressed as [34, 63]

$$\begin{aligned} \rho_M(\vec{r})&=\rho_{0M}(1+\omega r^2)\exp(-\beta r^2) \\ \rho_\alpha(\vec{r})&=\rho_{0\alpha}\exp(-\beta r^2). \end{aligned} \quad (6)$$

The parameters ρ_0, ω, β and the rms radii were taken from Ref. [20] and are given in Table 1. As reported in Ref. [34], $\beta=1/a^2$ and $\omega=\alpha/a^2$, where a is the length of the well and $\alpha=(Z-2)/3$ (Z is the proton number of the nucleus) [64]. The DFC potential was chosen to describe the nuclear potential because it takes into account the alpha clustering effects in the nuclei and such an approach is well suited for the ^{12}C nucleus. The plotted proximity and DFC potentials used in our calculations are shown in Fig. 1.

Table 1. Parameters of the nuclear matter densities and rms radii of ^{4}He and ^{12}C nuclei [20].

nucleus	ρ_0/fm^{-3}	ω/fm^{-2}	β/fm^{-2}	$\langle r^2\rangle^{1/2}$/fm
^{4}He	0.4229	0	0.7024	1.461
^{12}C	0.1644	0.4988	0.3741	2.407

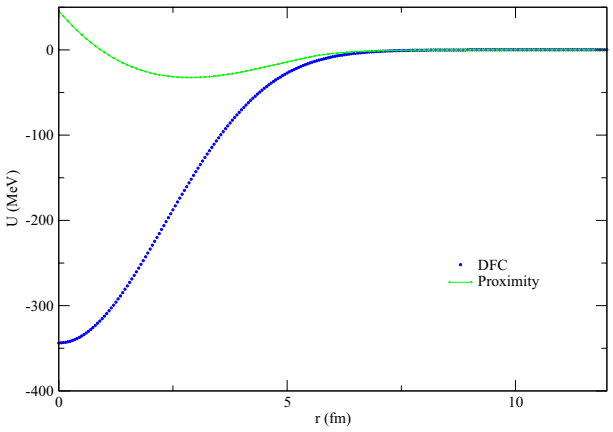

Fig. 1. (color online) Nuclear proximity and DFC potentials as a function of radius, as used in the calculations.

2.2 WKB Model

With the proximity and DFC potentials, astrophysical S-factor data for the ^{12}C+^{12}C reaction have been obtained in the framework of the WKB model. In calculations of decay, fusion and capture reaction observables, the WKB approximation is widely used [28, 31, 65]. To obtain the fusion cross section, first the transmission coefficient through a barrier generated by the effective potential between colliding nuclei needs to be calculated. The effective potential has three parts and it is given by:

$$V_{\rm eff}(r)=V_N(r)+V_C(r)+V_L(r), \quad (7)$$

where $V_N(r)$, $V_C(r)$ and $V_L(r)$ are the nuclear, Coulomb and centrifugal parts, respectively. The nuclear and Coulomb potentials are introduced in Sections 2.1 and 2.3 respectively. The Langer-modified centrifugal part is as follows [66]:

$$V_L(r)=\frac{\hbar^2}{2\mu}\frac{(l+1/2)^2}{r^2}, \quad (8)$$

where μ is the reduced mass and the transmission coefficient is given by

$$T_l(E)=4\left(2\theta+\frac{1}{2\theta}\right)^{-2}, \quad (9)$$

$$\theta=exp\left[\int_{r_1}^{r_2}\kappa(r)\mathrm{d}r\right], \kappa^2(r)=\frac{2\mu}{\hbar^2}[V_{\rm eff}-E]>0, \quad (10)$$

where r_1 and r_2 are the turning points. So the fusion cross section can be calculated as follows:

$$\sigma_f=\frac{\pi}{k^2}\sum_l(2l+1)T_l(E), \quad (11)$$

where $k^2=\frac{2\mu E}{\hbar^2}$ and E is the center-of-mass energy [28]. The modified astrophysical S-factor, which changes

smoothly with energy, can be calculated by using the following equation [6, 15]:

$$S^*(E)=\sigma_f(E)E\exp\left(\sqrt{\frac{E_g}{E}}+gE\right), \tag{12}$$

where g=0.46 MeV^{-1} and E_g is given by

$$E_g=986.4\text{ keV}\left((\frac{\mu}{m_p})(Z_1Z_2)^2\right), \tag{13}$$

where μ, m_p and Z_i are the reduced mass, mass of the proton and proton number of the target and projectile, respectively [10, 27, 34, 35].

2.3 Screening conditions

Thermonuclear reactions in stars are quite sensitive to the quantum tunneling process. In that case any modification on the Coulomb potential would affect the reaction observables, due to the change of the barrier of the effective potential between interacting nuclei. In a stellar environment, free electrons in the plasma and ions can attract each other, so electrons can form a cloud around the nuclei and isolate them. Therefore nuclear reactions in the stellar plasma are affected by this shielding. Screening depends on the thermal and density conditions of the plasma and it is treated as three regimes; weak, intermediate and strong. These regimes are identified by comparing the Coulomb energy E_c to thermal energy kT. If E_c is smaller than kT, it is called weak screening. If E_c is larger than kT, it is strong screening. The last regime, intermediate screening, is when $E_c\sim kT$ [36, 42]. With these screening effects, the Coulomb potential is decreased and needs to be modified with extra terms depending on the type of plasma. In this paper, the more general potential (MGECSC potential), which can be used to describe both Debye and quantum plasma conditions, has been chosen in order to investigate the screening effect. The pure Coulomb potential is given by:

$$\begin{aligned} V_C(r)&=\frac{Z_1Z_2e^2}{r}, && r\geqslant R_c\\ &=\frac{Z_1Z_2e^2}{2R_c}\left(3-\frac{r^2}{R_c^2}\right), && r<R_c, \end{aligned} \tag{14}$$

where Z_i, e and R_c are the charge of the interacting particle, elementary charge and Coulomb radius respectively. The shape of the MGECSC potential is as follows:

$$V(r)=\frac{Z_1Z_2e^2}{r}(1+br)\exp(-r/\lambda_D)\cos(cr/\lambda_D), \tag{15}$$

where b, c and λ_D are screening parameters. This potential has been introduced to investigate the electron screening effect on hydrogen atoms in a plasma and it is noted that MGECSC potential exhibits a stronger screening effect than other screening potentials [56]. If the quantum properties of the particles affect the plasma, the plasma can be considered a quantum plasma. Using the parameter c in the MGECSC potential, one can define Debye and quantum plasmas. This potential can also be reduced to the screened Coulomb potential (SC), exponential cosine screened Coulomb potential (ECSC) and pure Coulomb potential (PC). While parameter $c\neq0$ (this activates the cosine term), parameter b can be used to obtain much stronger screening, and b can also be used in the Debye plasma case (c=0) where it contributes the screening by a factor (1+br). Different potential barrier shapes for different b and c parameters can be found in Fig. 2. It can be seen that screening becomes much stronger in case of $b\neq0$ and $c\neq0$, and it should be noted that the greater contribution to the screening is provided by the cosine term, because the cosine term has an effect on the tail part of the potential barrier. It causes strong enhancement of the cross section especially at low energies, and dominates the observables. In Fig. 2, the proximity potential has been used for the nuclear part of the effective potential and it should be noted that we have performed all our calculations for s-wave. Another parameter in the MGECSC potential is the λ_D Debye screening length, given by:

$$\lambda_D=\sqrt{\frac{\epsilon_o k_b T}{n_e e^2}}, \tag{16}$$

where k_b, T, n_e, e and ϵ_o are the Boltzmann constant, plasma temperature, electron density, electron charge and dielectric constant, respectively. λ_D has units of length. More detailed information about the MGECSC potential can be found in Refs. [56, 57].

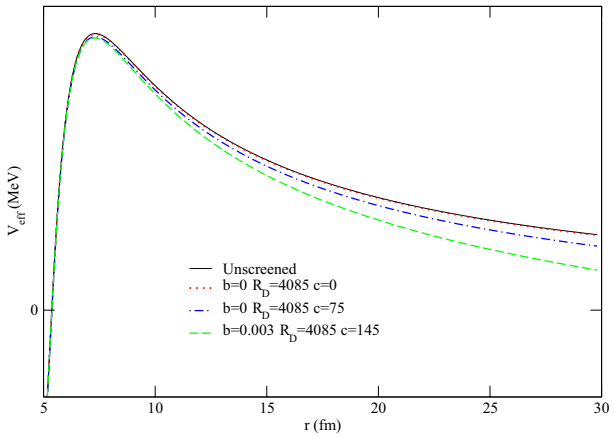

Fig. 2. (color online) Four different effective potentials as a function of radius. One is unscreened (solid line), and the others represent the screened cases with the MGECSC potential.

The weak screening conditions for the ^{12}C+^{12}C reaction are examined as follows. For a nonresonant ^{12}C+^{12}C fusion reaction in a nondegenerate plasma (electron degeneracy factor θ_e=1, mass fractions of the elements,

temperature and density conditions have been taken from Ref. [5]), the weak screening case satisfies:

$$T \gg 10^5 \rho^{1/3} \zeta^2, \tag{17}$$

where T is the temperature in kelvin, ρ is density in gcm^{-3} and ζ is defined as:

$$\zeta \equiv \sqrt{\sum_i \frac{(Z_i^2 + Z_i\theta_e)X_i}{A_i}}, \tag{18}$$

where Z_i, A_i and X_i are the proton number, mass number and mass fraction respectively of the related nuclei. ζ is associated with the Debye-Hückel radius and this radius is given by

$$R_D = \sqrt{\frac{kT}{4\pi e^2 \rho N_A \zeta^2}} = 2.812x10^{-7} \rho^{-1/2} T_9^{1/2} \zeta^{-1} \text{ cm}. \tag{19}$$

Equation (19) is the same parameter as given by Eq. (16). To calculate Eqs. (17), (18) and (19) we have used the hydrostatic carbon burning phase conditions of ρ=10^5 gcm^{-3} and $T = 0.9$ GK, and the mass fractions are assumed as $X^0_{^{12}\text{C}}$=0.25, $X^0_{^{16}\text{O}}$=0.73, $X^0_{^{20}\text{Ne}}$=0.01, $X^0_{^{22}\text{Ne}}$=0.01 [4, 5]. Under these conditions, Eq. (17) has been found to give 0.0197928 GK. This value is smaller than the 0.9 GK so the weak screening case is ensured despite the high density. The Debye-Hückel radius is found to be 4085 fm, from which the electron screening correction factor can be calculated as 1.17784, similar to the value given in Ref. [5]. However, we have used the obtained numerical Debye-Hückel radius value in Eq. (15) to modify the Coulomb potential. So we have calculated the fusion reactions observables (cross-sections and astropyhysical S-factors) in terms of obtained numerical values from the weak screening conditions, thus obtaining theoretical results can be compared with the experimental data.

3 Results and discussion

With the aim of determining a nuclear potential which is successful in explaining both the structure and fusion observables, we have applied the two different potentials to obtain better values for the nuclear structure observable, the cluster states of ^{24}Mg. The normalized resonant energy states of ^{24}Mg have been investigated for the $G = 16$ and $G = 18$ cluster bands. To calculate the normalized resonant energy states, the Gamow code [69] has been used with the DFC nuclear potential. The normalized resonant energy states have been calculated as follows:

$$\varepsilon = \frac{E(J^+) - E(0^+)}{E(2^+) - E(0^+)}. \tag{20}$$

The obtained results are shown in Fig. 3. The DFC potential including clustering effects in ^{12}C gives the cluster states of ^{24}Mg. After investigating the structure observables we have made a comparison between nuclear potentials, so we have calculated the astrophysical S-factor of ^{12}C+^{12}C in the framework of the proximity and DFC potentials with the WKB method. Our results can be divided into two subgroups: unscreened and screened cases for the proximity and DFC potentials.

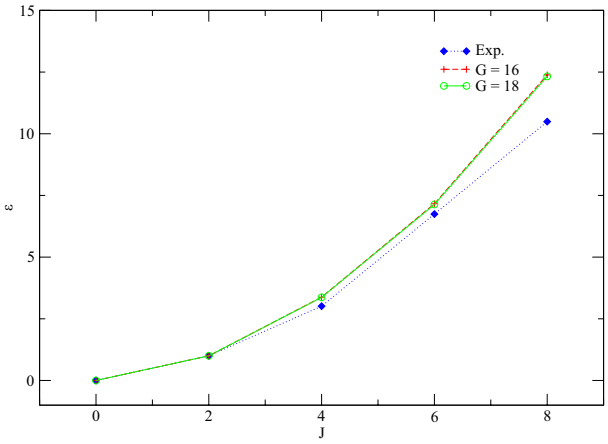

Fig. 3. (color online) Normalized resonant energy states of ^{24}Mg. Experimental data have been taken from Ref. [70]. The DFC potential for ^{12}C+^{12}C was used to obtain the resonant energy states of ^{24}Mg for the G=16 and 18 cluster bands.

Firstly, to investigate the influence of the screening parameters, we have used the MGECSC potential instead of the Coulomb potential. How effective potential and turning points change with different cases of MGECSC potential are presented in Fig. 2. In Fig. 2 the unscreened case has been plotted with three different cases of the MGECSC potential. The Coulomb barrier is almost unchanged in the "b=c=0 R_D=4085" case. Together with the activation of the parameters b and c, the screening has begun to be monitored more effectively and it is possible to say that the c parameter (cosine term) is more dominant in describing screening.

After investigating the barrier, we have performed unscreened and "R_D=4085 $c = 0$ $b = 0$" cases for both nuclear potential. As seen in Fig. 4, the behaviours of the two potentials are almost the same. Enhancement in the theoretical data is so small for "R_D=4085 c=0 b=0" because the cross sections are strictly related to the inner and outer turning points, according to Eq. (10), and one can understand from Fig. 2 that the turning points for "R_D=4085 $c = 0$ $b = 0$" are almost the same as the unscreened case. For this reason we have tested some numerical values that will help us explain the experimental cross sections and astrophysical S-factor data of the ^{12}C+^{12}C reaction. So we have used different forms of the MGECSC potential.

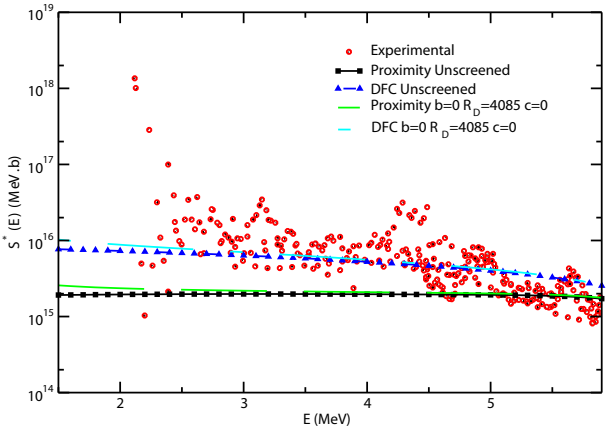

Fig. 4. (color online) Unscreened and b=c=0 cases for proximity and DFC potentials. The experimental data are from Refs. [6–15].

Thus, in addition to the $b=c=0$ case, the "$b=0$ c=75" and "b=0.003 c=145" cases have also been examined for the proximity potential and as seen in Fig. 5, the results reveal the contribution of the cosine term to the screening. Following the proximity potential, the procedure has been repeated for the DFC potential. The unscreened, "b=c=0", "b=0 c=45" and "b=0.01 c=160" cases are presented in Fig. 6. To compare semi-classical results we have repeated the DFC potential calculations with the CCfull code [67], and the results can be seen in Fig. 7. In the CCfull calculations we have had to neglect the g factor in the expression of the S factor. Otherwise the astrophysical S-factor data could not be produced properly. As seen in Fig. 7, the screening parameters used in the WKB model have also been used for the CCfull calculations. In total we have performed ten cases for all potentials and calculation methods. The potential types and parameters used can be found in Table 2.

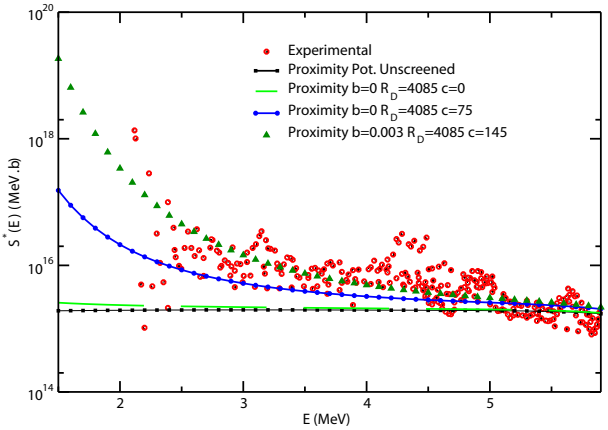

Fig. 5. (color online) Comparison of the unscreened and screened cases in terms of astrophysical S-factors of ^{12}C+^{12}C fusion for the proximity potential. The experimental data are from Refs. [6–15].

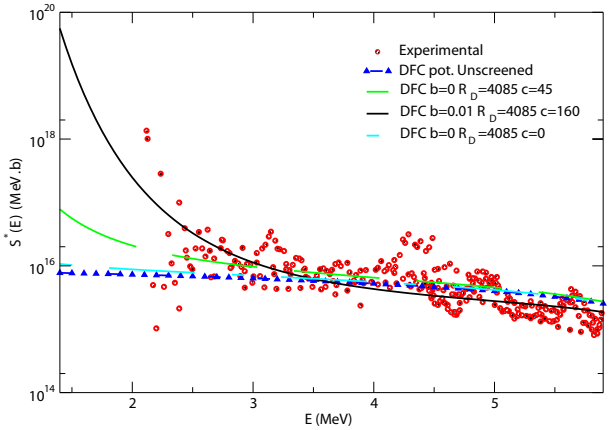

Fig. 6. (color online) Comparison of the unscreened and screened cases in terms of astrophysical S-factors of ^{12}C+^{12}C fusion for the DFC potential. The experimental data are from Refs. [6–15].

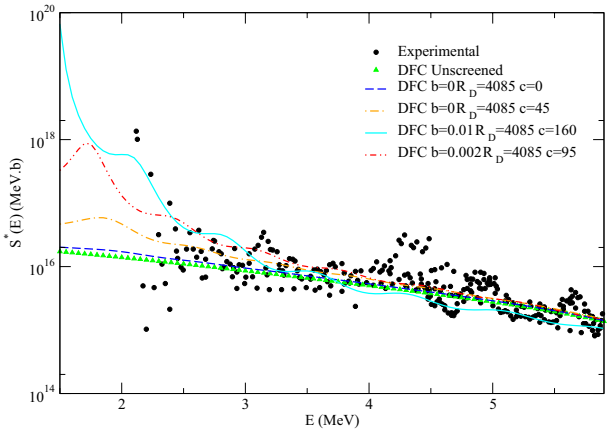

Fig. 7. (color online) Predictions of ^{12}C+^{12}C astrophysical S-factor with DFC potential and four electron screening cases. CCfull code has been used in the calculations. The experimental data are from Refs. [6–15].

Table 2. The electron screening parameters used in the WKB and coupled channel (CC) calculations.

potential types	b	c	R_D	method
Prox 77	0.00	0	4085	WKB
Prox 77	0.00	75	4085	WKB
Prox 77	0.003	145	4085	WKB
DFC	0.00	0	4085	WKB
DFC	0.00	45	4085	WKB
DFC	0.01	160	4085	WKB
DFC	0.00	0	4085	CC
DFC	0.00	45	4085	CC
DFC	0.01	160	4085	CC
DFC	0.002	95	4085	CC

4 Conclusion

In this paper, we have investigated the astrophysically important ^{12}C+^{12}C fusion reaction in the framework of the proximity and DFC potentials. First, the resonant energy states of ^{24}Mg for the G=16 and G=18 cluster bands have been investigated with the proximity and DFC potentials between ^{12}C nuclei to find which potential best describes the structure observables. According to the obtained results, the DFC potential is the most successful, while reasonable results could not obtained with the proximity potential. This shows that the DFC potential considering the clustering effects in ^{12}C produces much better results for the cluster states of ^{24}Mg. Another characteristic difference between these two potentials is their depth.

Astrophysical S-factors have been produced with both the proximity and DFC potentials. It can be said that the microscopic DFC potential is more appropriate than the phenomenological proximity potential to explain the ^{12}C+^{12}C fusion observables. But, even if the nuclear potentials differ in describing experimental data, the same behavior has been observed for both of them. As known fusion reactions in stars occur at small energies, for this reason they are quite sensitive quantum tunnelling processes which are related to the Coulomb barrier. So any modification to the Coulomb potential because of the external conditions affects the reaction observables directly. In this way, we have investigated the electron screening effect on the ^{12}C+^{12}C fusion reaction in the framework of the weak screening case. Despite the high density, the obtained numerical values show that the ^{12}C+^{12}C fusion reaction remains within the weak screening limits. In the calculations of weak screening conditions, density and temperature have been chosen for hydrostatic carbon burning. In this way, the obtained R_D value has been used in the screening calculations.

First, we checked the classical screening case with obtained R_D ($b=c=0$) value for both nuclear potentials. The shift in the barrier is so small when $b=c=0$ and R_D=4085 that only small changes have been observed in the S-factor data. So in order to produce better results, the MGECSC potential has been included to our calculations for the ^{12}C+^{12}C fusion reaction and these modifications have been improved the theoretical results. We have chosen two cases for two potentials in WKB calculations. For the proximity potential the "b=0 c=75" and "b=0.003 c=145" cases have been used and the behavior of the theoretical results is nearly the same up to 4 MeV. While approaching small energies, the "b=0.003 c=145" case shows a dramatic increase. The "b=0 c=45" and "b=0.01 c=160" cases have been performed for the DFC potential in the WKB method. The "b=0 c=45" case has little difference from the unscreened and "b=c=0" cases above 4 MeV. The "b=0.01 c=160" case has good agreement with the experimental data in comparison to the others. In addition to the "b=0.002 c=95" case, the cases which were used for the DFC potential in WKB calculations have also been used for CCfull calculations. Slightly below 2 MeV a weak oscillation appears when we set the values "b=c=0" and it becomes more visible and stronger with increasing c value for the CCfull calculations. In understanding the results for both calculation methods, the c parameter (in an other words the cosine term) dominates the behaviours of the models. Besides, it is possible to get similar results with uses of the different R_D values (R_D<<4085). When the R_D is chosen smaller than the specified value, however, weak screening rules cannot be applied for the reaction of interest.

In conclusion, it should be noted that considering the screening effects with the MGECSC potential is important for explaining the ^{12}C+^{12}C nuclear fusion data. The microscopic DFC potential is better than the proximity potential in explaining the experimental data, also taking into account that clustering effects are dominant for the structure of ^{24}Mg nuclei. The MGECSC potential causes a very strong screening effect especially at low energies, and the theoretical results show that the MGECSC potential provides much higher enhancement factors than the normal screening potentials.

References

1 E. G. Adelberger, S. M. Austin, J. N. Bahcall et al, Rev. Mod. Phys., **70**(4): 1265 (1998)
2 E. G. Adelberger, A. Garca, R. G. H. Robertson et al, Rev. Mod. Phys., **83**(1): 195 (2011)
3 D. D. Clayton, *Principles of stellar evolution and nucleosynthesis*, University of Chicago Press Edition (Chicago, USA, University of Chicago Press, 1983), p. 430
4 D. Arnett, *Supernovae and nucleosynthesis* , First Edition (New Jersey, Princeton, Princeton University Press, 1996), p. 75
5 C. Illiadis, *Nuclear Physics of Stars*, Second, Revised and Enlarged Edition (Weinheim, Germany, Wiley-VCH Verlag GmbH & Co., 2015), p. 400
6 J. R. Patterson, H. Winkler, and C. S. Zaidins, Astrophys. J., **157**: 367 (1969)
7 M. G. Mazarakis, and W. E. Stephens, Phys. Rev. C, **7**(4): 1280 (1973)
8 M. D. High, and B. Cujec, Nucl. Phys. A, **282** (1): 181-188 (1977)
9 K. A. Erb, R. R. Betts, S. K. Korotky et al, Phys. Rev. C, **22**(2): 507 (1980)
10 K. U. Kettner, H. Lorenz-Wirzba and C. Rolfs, Z. Phys. A, **298**(1): 65-75 (1980)
11 H. W. Becker, K. U. Kettner, C. Z. Rolfs et al, Z. Phys. A, **303**(4): 305-312 (1981)
12 B. Dasmahapatra, B. Cujec, and F. Lahlou, Nucl. Phys. A, **384**(1-2): 257-272 (1982)
13 L. J. Satkowiak, P. A. DeYoung, J. J. Kolata et al, Phys. Rev.

C, **26** (5): 2027 (1982)
14 L. Barron-Palos, E. F. Aguilera, J. Aspiazu et al, Nucl. Phys. A, **779**: 318-332 (2006)
15 T. Spillane, F. Raiola, C. Rolfs et al, Phys. Rev. Lett., **98**(12): 122501 (2007)
16 F. Strieder, (In: Journal of Physics: Conference Series. IOP Publishing, 2010), p. 012025
17 X. Fang, B. Bucher, S. Almaraz-Calderon et al, (In: Journal of Physics: Conference Series. IOP Publishing, 2013), p. 012151
18 D. Santiago-Gonzales, (In: EPJ Web of Conferences. EDP Sciences, 2016), p. 09011
19 R. Kippenhahn, A. Weigert and A. Weiss, *Stellar Structure and Evolution*, Second Edition (Heidelberg, Berlin, Springer-Verlag, 2012), p.199
20 A. A. Aziz, N. Yusof, M. Z. Firihu et al, Phys. Rev. C, **91**(1): 015811 (2015)
21 W. D. Arnett and J. W. Truran, Astrophys. J., **157**: 339 (1969)
22 F. Strieder, J. Phys. G: Nucl. Part. Phys., **35**(1): 014009 (2007)
23 E. F. Aguilera, P. Rosales, E. Martinez-Quiroz et al, Phys. Rev. C, **73**(6): 064601 (2006)
24 C. L. Jiang et al. , Phys. Rev. Lett., **110**(7): 072701 (2013)
25 A. Diaz-Torres and M. Wiescher, (In: Journal of Physics: Conference Series. IOP Publishing, 2014), p. 012006
26 A. Diaz-Torres and M. Wiescher, (In: EPJ Web of Conferences. EDP Sciences, 2015), p. 02017
27 V. Y. Denisov, and N. A. Pilipenko, Phys. Rev. C, **81**(2): 025805 (2010)
28 Q. Haider, J. Y. Shapiro and A. Sharma, II Nuovo Cim. A (1965-1970), **106**(3): 343-354 (1993)
29 F. Koyuncu and A. Soylu, Int. J. Mod. Phys. E, **26**(12): 1750086 (2017)
30 F. Koyuncu, A. Soylu, and O. Bayrak, Mod. Phys. Lett. A, **32**(09): 1750050 (2017)
31 V. Y. Denisov, and H. Ikezoe, Phys. Rev. C, **72**(6): 064613 (2005)
32 V. Y. Denisov, and A. A. Khudenko, Phys. Rev. C, **80**(3): 034603 (2009)
33 D. L. Hill, and J. A. Wheeler, Phys. Rev., **89**(5): 1102 (1953)
34 G. Kocak, M. Karakoc, I. Boztosun et al, Phys. Rev. C, **81**(2): 024615 (2010)
35 R. Kunz, M. Fey, M. Jaeger et al Astrophys. J., **567**: 643-650 (2002)
36 E. E. Salpeter, Aust. J. Phys., **7**(3): 373-388 (1954)
37 M. Lattuada, R. G. Pizzone, S. Typel et al, Astrophys. J., **562**(2): 1076 (2001)
38 K. Czerski, A. Huke, A. Biller, et al, Europhys. Lett., **54**(4): 449 (2001)
39 P. Quarati, and A. M. Scarfone, Astrophys. J., **666**(2): 1303 (2007)
40 H. E. Dewitt, H. C. Graboske and M. S. Cooper, Astrophys. J., **181**: 439-456 (1973)
41 H. C. Graboske, H. E. Dewitt, A. S. Grossman et al., Astrophys. J.,**181**: 457-474 (1973)
42 R. K. Wallace, S. E. Woosley and T. A. Weaver, Astrophys. J., **258**: 696-715 (1982)
43 C. Carraro, A. Schäfer and S. E. Koonin, Astrophys. J., **331**: 565-571 (1988)
44 A. V. Gruzinov and J. N. Bahcall, Astrophys. J., **504**: 996-1001 (1998)
45 L. R. Gasques, A. V. Afanasjev, E. F. Aguilera et al, Phys. Rev. C, **72**(2): 025806 (2005)
46 H. J. Assenbaum, K. Langanke, and C. Rolfs, Z. Phys. A, **327**(4): 461-468 (1987)
47 T. E. Liolios, Phys. Rev. C, **61**(5): 055802 (2000)
48 R. L. Cooper, A. W. Steiner, and E. F. Brown, Astrophys. J., **702**(1): 660 (2009)
49 C. Spilateri, C. A. Bertulani, L. Fortunato et al, Phys. Lett. B **755**: 275-278 (2016)
50 M. A. Famiano, A. B. Balantekin and T. Kajino, Phys. Rev. C, **93** (4): 045804 (2016)
58 X. Yao, T. Mehen and B. Müller, Phys. Rev. C, **95**(11): 116002 (2017)
52 Y. H. Chen, MNRAS, **475**(1): 20-26 (2018)
53 B. Saha, P. K. Mukherjee, and G. H. Diercksen, Astron. Astrophys., **396**(1): 337-344 (2002)
54 P. K. Shukla and B. Eliasson, Phys. Lett. A, **372**: 2897-2899 (2008)
55 S. Paul and Y. K. Ho, Comput. Phys. Commun., **182**: 130133 (2011)
56 A. Soylu, Phys. Plasmas, **19**(7): 072701 (2012)
57 M. K. Bahar, and A. Soylu, Phys. Plasmas, **21** (9): 092703, (2014)
58 G. L. Zhang, Y. J. Yao, M. F. Guo et al, Nucl. Phys. A, **951**: 86-96 (2016)
59 I. Dutt, and R. K. Puri, Phys. Rev. C, **81**(6): 064609 (2010)
60 J. Blocki, J. Randrup, W. J. Swiatecki et al, Ann. Phys., **105**(2): 427-462 (1977)
61 B. Bucks, H. Friedrich, and C. Wheatley, Nucl. Phys. A, **275**(1): 246-268 (1977)
62 M. E. A. Farid, Z. M. M. Mahmoud, and G. S. Hassan, Phys. Rev. C, **64**(1): 014310 (2001)
63 G. R. Satchler, and W. G. Love, Physics Reports, **55**(3): 183-254 (1979)
64 H. F. Ehrenberg et al., Phys. Rev., **113**: 666 (1959)
65 A. Soylu, and O. Bayrak, Eur. Phys. J. A, **51**(4): 46 (2015)
66 R. E. Langer, Phys. Rev., **51**(8): 669 (1937)
67 K. Hagino, N. Rowley, and A. T. Kruppa, Comput. Phys. Commun., **123**(1-3): 143-152 (1999)
68 S. E. Woosley, A. Heger, and T. A. Weaver, Rev. Mod. Phys., **74**(4): 1015 (2002)
69 T. Vertse, K. F. Pal, and Z. Balogh, Comput. Phys. Commun., **27**(3): 309-322 (1982)
70 B. Buck, P. D. B. Hopkins, and A. C. Merchant, Nucl. Phys. A, **513**(1): 75-114 (1990)